Characterization and production of agglomerated cork stoppers for spirits based on a factor analysis method

M. Suffo [a,*], D.L. Sales [b], E. Cortés-Triviño [c], M. de la Mata [b], E. Jiménez [d]

[a] *Department of Mechanical Engineering and Industrial Design, High Engineering School, Universidad de Cádiz, Campus Río San Pedro s/n, 11510 Puerto Real, Cádiz, Spain*
[b] *Departamento de Ciencia de los Materiales e Ingeniería Metalúrgica y Química Inorgánica, IMEYMAT, Universidad de Cádiz, Campus Río San Pedro, 11510 Puerto Real, Cádiz, Spain*
[c] *Departamento de Ingeniería Química, Química Física y Ciencias de los Materiales, Centro de Investigación en Tecnológica de Productos y Procesos Químicos (Pro2Tecs), Escuela Técnica Superior de Ingeniería (ETSI), Campus del Carmen, Universidad de Huelva, 21071 Huelva, Spain*
[d] *R&D, Innovation and Engineering Company of Torrent Group, N-IV km 649, 11500 El Puerto Santa María, Cadiz, Spain*

ARTICLE INFO

ABSTRACT

The decision-making in the investment of a new line of stoppers based on agglomerated cork requires knowledge of the composition and its contribution to its performance. For this, it is necessary to observe the leading products on the market and to test a series of prototypes with different formulations. The development of manufacturing products made by cork, such as bottle stoppers, benefits strongly from accurate chemical and structural characterizations, correlated to the final material performance. A wise starting point to fulfill such requirement consist of comparing available products in the market to be compared with different prototypes with varying composition. This work presents a blind characterization of a series of cork samples through a non-supervised exploratory analysis designed to select agglomerated corks for spirits and still wines in the packaging industry. A total of 18 batches, with 3 of them being high-end commercial products, were used to build 15 different prototypes. They were subsequently characterized with the exact composition of microgranulated cork as the unknown variable. Statistical results based on 14 parameters related to the physic-thermo-mechanical properties indicate that the suitability of selecting the stopper relies on the study of only 4 or 5 of the initial parameters. Hence, it is shown that a reduced number of parameters may be considered to properly describe the mechanical behavior of agglomerated cork, allowing the wise choice of the most convenient material for the intended application. The factorial map reveals that the only sample batch manufactured based on the tested prototypes correlates with the three of the products supplied by the competence.

1. Introduction

Natural cork is a cellular, light, renewable and biodegradable material that is extracted directly from the oak tree (*Quercus suber L*) approximately every 9 years. Its composition is well known and its maintenance contributes markedly to the ecosystem preservation (Mestre & Vogtlander, 2013; Pacheco Menor, Serna Ros, Macías García, & Arévalo Caballero, 2019; Gil, 2015).

The production of agglomerated cork (AC) stoppers for the wine sector (spirits and still wines) is concentrated in several countries of Southern Europe (Spain, Portugal, and Morocco), as they rely on raw material in origin to acquire the natural cork (Rives, Fernandez-Rodriguez, Rieradevall, & Gabarrell, 2011; Rives,

Fernández-Rodríguez, Rieradevall, & Gabarrell, 2012). These countries account for 50% of the world's cork production as they host a third of the world's oak tree surface (Gil, 2009, 2015). Half of the cork produced in Spain is extracted from the Reserve of oak trees of the Iberian Peninsula (Los Alcornocales Natural Park), with about 78,000 tons per year, an amount that is only surpassed by the neighboring country of Portugal (González-Hernández, González-Adrados, García De Ceca, & Sánchez-González, 2014).

The morphology and mechanical properties of the AC for stoppers have been widely described for more than 50 years (Natividade, 1950; Guillemonat, 1960; Pereira, 1988; Silva et al., 2005; Pérez-Terrazas, González-Adrados, & Sánchez-González, 2020; Urion, Bellat, Liger-Belair, Gougeon, & Karbowiak, 2021). However, no records have been found on the percentages of each component that conforms to a

---

* Corresponding author.
E-mail address: miguel.suffo@uca.es (M. Suffo).

Nomenclature			Total Reflectance	
		δ	Loss factor, dimensionless	
AC	Agglomerated cork	**H**	Humidity, %	
D	Apparent density, kg/m^3	**ICCSMP**	International Code of Cork Stopper Manufacturing Practices	
d	Average diameter, mm			
$\boldsymbol{\sigma_m}$	Ultimate strength, MPa	**l**	length, mm	
$\boldsymbol{\sigma_{50}}$	Compressive strength at 50% strain, MPa	**m**	mass, g	
$\boldsymbol{\sigma_{23}}$	Compressive strength at 23% strain, MPa	**M**	moment of torsion at break, daN·cm	
$\boldsymbol{\sigma_{34}}$	Compressive strength at 34% strain, MPa	**Py-GC-MS**	Pyrolysis Gas Chromatography Mass Spectrometry	
$\boldsymbol{\rho_{ap}}$	Apparent density, kg·cm^{-3}	**θ**	Torsion angle at break, rad	
$\boldsymbol{\rho_t}$	True density, kg·cm^{-3}	$\mathbf{T_s}$	Shear stress at break, daN/cm^2	
DSC	Differential scanning calorimetry	**SEM**	Scanning Electron Microscopy	
DTMA/DMA	Dynamic Thermal Mechanical Analysis	**t**	time, min	
EDX	Energy-dispersive X-ray spectroscopy	**T**	Temperature, ºC	
$\mathbf{E_c}$	Youngś modulus (determined in compression test), MPa	$\mathbf{T_m}$	Melting temperature, ºC	
$\mathbf{E_t}$	Youngś modulus (determined in tensile test), MPa	**ΔH**	Enthalpy rate, J/g	
$\boldsymbol{\varepsilon_m}$	Strain at strength, MPa	**ε**	Strain, %	
$\boldsymbol{\varepsilon_{tb}}$	Strain at break, MPa	$\boldsymbol{\varepsilon_b}$	Strain at break, %	
E'	Storage modulus, MPa	**σ**	Stress, MPa	
E''	Loss modulus, MPa	$\boldsymbol{\sigma_b}$	Stress at break, %	
FTIR-ATR	Fourier Transform Infrared Spectroscopy – Attenuated			

certain differential behavior.

In a similar way to the epithelial tissue or the trabecular bone, one of the most outstanding properties that give the cork its closed-cell structure is the viscoelasticity that in turn determines the resilience level (Hejnowicz & Sievers, 1996; González-Hernández et al., 2014). The heterogeneity of the internal structure of the AC caused during the manufacturing process causes a great uncertainty when its behavior is studied in relation to the orientations in which the external loads derived from the normal operation are applied (Delucia, Catapano, Montemurro, & Pailhés, 2020; Anjos, Pereira, & Rosa, 2011). M. Rosa & Fortes (1993) already highlighted the importance of anisotropy, a physical-mechanical property of cork that will be transferred to the overall system, either naturally or as an agglomerate (Silva et al., 2005). Nevertheless, AC in stoppers presents randomly oriented cork domains, hence resulting in a more isotropic behavior (Paiva & Magalhães, 2018; Oliveira, Knapic, & Pereira, 2015).

As indicated, AC is a composite material benefiting from the amphoteric properties of natural cork (Silva et al., 2005). They mix well with binder polymers to obtain stoppers elastic enough to withstand the compression, traction, and torsion loads associated with the processes of opening, closing, and manipulation during the cork introduction in the neck of the bottle (Sánchez-González & Pérez-Terrazas, 2018). Some authors have shown promising results on resilient materials by using quasi-static (Fernandes, Correlo, Mano, & Reis, 2014) dynamic-mechanical tests (DTMA) (Mano, 2002; Gameiro, Cirne, Gary, & Al, 2005; Policarpo, Neves, & Maia, 2014; Paiva & Magalhães, 2018). However, their studies also highlighted the uncertainty associated to these materials and the need to characterize them through complementary hybrid techniques to understand the properties required for a new product prototype to be launched on the market.

Currently, microgranulated cork agglomerate is replacing natural cork in wine stoppers but every manufacturer applies a secret composition, with the percentage of each basic constituent being approximately estimated by the following:

A% polyurethane adhesives, according Franken, Primke, and Alvaro (2003).
B% thermoplastic expander polymer microspheres (usually PE).
C% lubricant (silicone, latex, etc.), this component is the one with the smallest proportion.

Rest: ≥ 75%microgranules of natural cork, as a mixture of 0.5–2 mm granulometry, according to International Code of Cork Stopper Manufacturing Practices (ICCSMP).

Combining these constituents, the ratios providing the cork its special utility as a stopper and particular exclusivity for each producer are obtained. The relationship between cork density and porosity, related to Young's modulus, and the stresses at different deformations, have been studied for three natural corks with different densities (high, medium and, low) (Pereira, 1988; Anjos, Pereira;, & Rosa., 2010). Although there are previous studies on AC for sparkling and still wines (Pereira, 2011; Urion et al., 2021; Fernandes et al., 2014; Gameiro et al., 2005), Spirit wines are usually consumed in a different way than the first ones, that is, they are not usually consumed at the same moment that the bottle has been opened, that is why the stopper undergoes more work cycles.

Currently, high uncertainty is still present during the decision-making process to define the parameters that better characterize the material depending on the type of cork, extraction origin, type of stopper, type of wine or oil, and nature of natural cork, as too many variables must be used to standardize a universal characterization method. (Rocha, Ganito, Barros, Carapuça, & Delgadillo, 2005) used statistical tools to provide reliable insights in order to determine if the cork stoppers were able to contaminate a wine: nevertheless up to the end of our knowledge, no methodologies have been reported that make it possible to clearly analyze which characteristics of microgranulated AC have a greater impact on its performance as a cork stopper in the premium sector of the spirits market.

In this work, we present a blind characterization where the composition is an unknown variable. We start the study with three samples (A, B, C) picked from commercial "premium" brands (aecork, 2017). To analyze 14 different variables, a series of chemical-physical-mechanical tests are applied both, at micro- and macro-structural levels, to a set of 18 sample batches of AC. The statistical exploration methodology based on unsupervised factor analysis technique will influence decision-making when selecting the prototype of AC stoppers for spirits and still wines that leads to the successful placing on the market by a local manufacturer whose brand of capsules and closures has been known for more than 100 years.

2. Material and methods

Table 1 summarizes the analyses performed, differentiating four

Table 1

List of samples studied and summary of the characterization performed to each one.

Sample photo and ID		D	H	M	S	C	T	To	V	F	PyM
		Characterization									
STAGE I. MARKET ANALYSIS											
	A	X	X	X	X	X	X	X	X	X	X
	B	X	X	X	X	X	X	X	X	X	X
	C	X	X	X	X	X	X	X	X	X	X
STAGE II. PROTOTYPING 1											
	P1	X	X	X	X	X	X	X	X		
	P2	X	X	X	X	X	X	X	X		
	P3	X	X	X	X	X	X	X	X		
	P4	X	X	X	X	X	X	X	X		
	P5	X	X	X	X	X	X	X	X		
STAGE III. PROTOTYPING 2											
	P6	X	X	X	X	X	X	X			
	P7	X	X	X	X	X	X	X			
	P8	X	X	X	X	X	X	X			
	P9	X	X	X	X	X	X	X			
	P10	X	X	X	X	X	X	X			
	P11	X	X	X	X	X	X	X			
	P12	X	X	X	X	X	X	X			
	P13	X	X	X	X	X	X	X			
	P14	X	X	X	X	X	X	X			
STAGE IV. PRODUCT VALIDATION											
	V1	X	X	X	X	X	X	X			

D: Density; H: Humidity; S: Microstructure (SEM); C: Compression; T: Tensile; To: Torsion; V: Viscoelasticity (DTMA); F: FTIR spectroscopy; PyM: Pyrolysis gas chromatography mass spectrometry.

different stages: market analysis, prototyping (two stages), and validation.

2.1. Materials

All the samples consist of AC containing a microgranulated cork with a granulometry between 0.5 and 2.0 mm (Oliveira, Furtado, Bastos, Guedes de Pinho, & Pinto, 2020).

For clarity, we establish four differentiated stages. Stage I refers to the study of commercial stoppers (high-end manufacturers), labeled as samples A, B, and C. The results are used to design the first five prototypes (stage II). Stages II and III focus on the design of prototypes with varying compositing based on the observed behavior of each component of the agglomerate. In these phases, a total of five and nine prototypes were manufactured respectively, suitable for a definitive product.

Stage IV concerns the manufacturing of the commercial products for spirits, still, and generous wines, successfully fulfilling the manufacturer requirements. The factor analysis of the product (V1) with all the tested samples allows comparing the characteristics of the product with the three references (A, B, C) from the statistical point of view.

2.2. Physical and chemical characterization

The physical characterization methods here described comply with the specific standards of the sector of cork stoppers for wines (UNE-EN 12726-2019).

2.2.1. Microstructural and chemical characterization

Fourier transform infrared spectroscopy – attenuated total reflectance (FTIR–ATR) is performed on the three reference samples of stage I to identify the constituents of the AC. This method provides information related to the presence or absence of specific functional groups, as well as the chemical structure of polymer materials, to take as a reference for the first formulations. This test is only carried out at this stage as the following batches are formulated based on the first ones. For this, a Bruker Vertex70 FTIR Spectrophotometer is used. It allows the recording of FTIR spectra of solid, liquid, and gaseous samples in the mid and near-infrared ranges. The samples did not undergo any preparation. For the acquisition of spectra, a standard spectral resolution of 4 cm^{-1} within the range of 4000–500 cm^{-1} was used, as well as 64 accumulations per sample. For this, a Golden Gate Single Reflection Diamond ATR System accessory has been used. The test was carried out on n = 3 replicas of each of the 3 batches: A, B, C. (Pacheco Menor et al., 2019). Second, the chemical analyses of constituents were continued to delve into those elements that could influence the series of physic-mechanical tests and distort the results.

Additionally, Stage I samples (A, B, C) were analyzed by Pyrolysis gas chromatography mass spectrometry (Py-GCMS). The results served to design the remaining samples (Stages II–IV). For this, an AcqMethod PY-Trinita DB1701 30 m has been used (Silva et al., 2005).

The materials were also analyzed by scanning electron microscopy (SEM) techniques to investigate the morphology of the materials at the micro / nano scale and the distribution of the phases forming the agglomerates. Images were acquired at x32, x120, and x500 magnifications using a FEI Nova NanoSEM microscope equipped with an X-ray detector.

2.2.2. Apparent density

The apparent density (n = 5) is determined according to the Spanish standard UNE 56922-2004 (UNE-EN 12726-2019) at one randomly selected sample of each batch. Mass measurements are carried out on a 0.001 g precision balance and the volume is calculated from their dimensional values, previously measured with a Vernier caliper. The calculation is carried out by applying the Eq. (1).

$$D = \frac{4 \cdot 10^6 \cdot m}{\pi \cdot d^2 \cdot l} \tag{1}$$

Where: D: apparent density in kg/m^3, rounded to the nearest unit (Anjos, Rodrigues, Morais, & Pereira, 2014).

m: mass in grams, rounded to 0.01 g d: calculated mean diameter l: length in mm, rounded to 0.1 mm.

2.2.3. Relative humidity

The test method to determine this property is based on the Spanish standards UNE 56917-88 and UNE 56922-2004. Similar to the previous analyses, 5 replicates (n = 5) of each batch, randomly selected, were characterized. A drying oven was used until constant weight. Humidity (H) is calculated as the loss of weight $(m_1 - m_2)$ over the mass after drying, m_2, by applying Eq. (2):

$$H = \frac{m_1 - m_2}{m_2} \cdot 100 \tag{2}$$

H in Eq. (2) is rounded to the nearest tenth of a percentage unit.

2.3. Mechanical tests

Specimens for mechanical testing are directly extracted in the stoppers length direction from the samples using cutting tools.

2.3.1. Uniaxial compression test

Uniaxial compression test is performed to n = 3 samples of each batch, randomly selected, following similar methodology explained in reference (Gybson, Easterling, & Ashby, 1981). The specimens were tested along its main longitudinal axis at a constant speed of 1 mm/s until 50 kN using a universal testing machine Shimadzu AG-X series at standard atmosphere (the temperature was 23 ± 2 °C and the relative humidity 50 ± 5%). During this procedure, the load sustained by the specimens and the elongation were measured. Young's modulus, E_c, is determined within the range of 2–4% of strain, where linear behavior is observed. Additionally, compressive strength, σ_{50}, and values of stress at 23% and 34% of strain, σ_{23} and σ_{34}, were determined. These later stress values are reference ones for stoppers, corresponding to the stress experienced by stoppers during bottling (Anjos et al., 2014; Lagorce-Tachon, Karbowiak, Champion, Gougeon, & Bellat, 2015).

2.3.2. Uniaxial tensile test

Similarly, uniaxial tensile tests are carried out to n = 3 samples of each batch. The samples were cut into a rectangular prism shape 5 mm thick, 14 mm wide, and 12 mm in calibrated length (the specimens have a length greater than the calibrated one to allow gripping). The standard UNE-EN ISO 527–4 is followed, being the deformation rate set at 2 mm/min during the test.

2.3.3. Torsion test

Torsion tests were performed in n = 5 samples, given the uncertainty presented by the trial and the lack of bibliographic references that provide information. The specimens were cut into cylinders of 5 mm diameter and variable length depending on the type of sample. The tests are carried out on a deformation rheometer controlled, Ares GII (TA Instruments, Inc.), using specific geometries for torsion tests with rectangular-type clamps. The specimens were fixed between the clamps with a 6.5 mm separation between them (distance between grips), remaining unchanged during the test. Rotational tests have been carried out at a speed of 4 rpm, as indicated by Spanish standards UNE 56923-2006. The results obtained from the different tests correspond to the replica that is closest to the calculated mean values.

2.3.4. Thermo-mechanical tests

Compression dynamic mechanical measurements were performed using a DMA Q800 (TA Instruments, Inc.) within the temperature range of −100, 100 °C. The temperature heating rate applied was 3 °C·min^{-1} and gaseous nitrogen was used to keep a controlled atmosphere inside of the sample container chamber during cooling and heating steps. Before the temperature ramp, the samples were stabilized and kept isothermally at −100 °C for 5 min. Specimens had a cylindrical shape 9,5 mm high and were tested at frequencies of 1 Hz. Experiments are carried out in mixed control with a preload of 0,3 N and a maximum sample amplitude of 50 μm and 0,70% strain. Storage modulus, E', loss modulus, $E'\prime$, and loss factor tan δ are obtained (Policarpo et al., 2014; Lagorce-Tachon et al., 2015; Paiva & Magalhães, 2018).

The methodology aims to establish a comparison of the elastic dynamic behavior of the samples in the first phases of the study in a wide temperature range. The samples with the lowest tanδ values for the temperatures selected as critical are identified to formulate prototypes (stages II and III) and, eventually, the final product.

The thermo-mechanical characterization is completed with DSC and TGA analyses. DSC measurements were carried out to stage I samples, following the ISO 11357 standard, in a Mettler Toledo (USA) DSC 1/200 equipment connected to a cryogenic device working between −35 ºC and 200 ºC. Every test requires a sample of approximately 6 mg, being subjected under the following experimental conditions: 10℃/*min* ramp and a N$_2$ purge gas flow rate of 50*ml/min*, to avoid oxidative or hydrolytic degradation during testing. The Thermogravimetric Analyses

were carried following the ISO 11358 standard out in a SDT Q600 thermobalance. Samples are heated up to 900 ºC at 20℃/*min,* in a flow of synthetic air (10*ml/min*).

2.4. Statistical analysis

The Factor Analysis (FA) (Xu, Huang, Liu, & He, 2019), as a statistical tool, was carried out to choose those parameters that clearly and

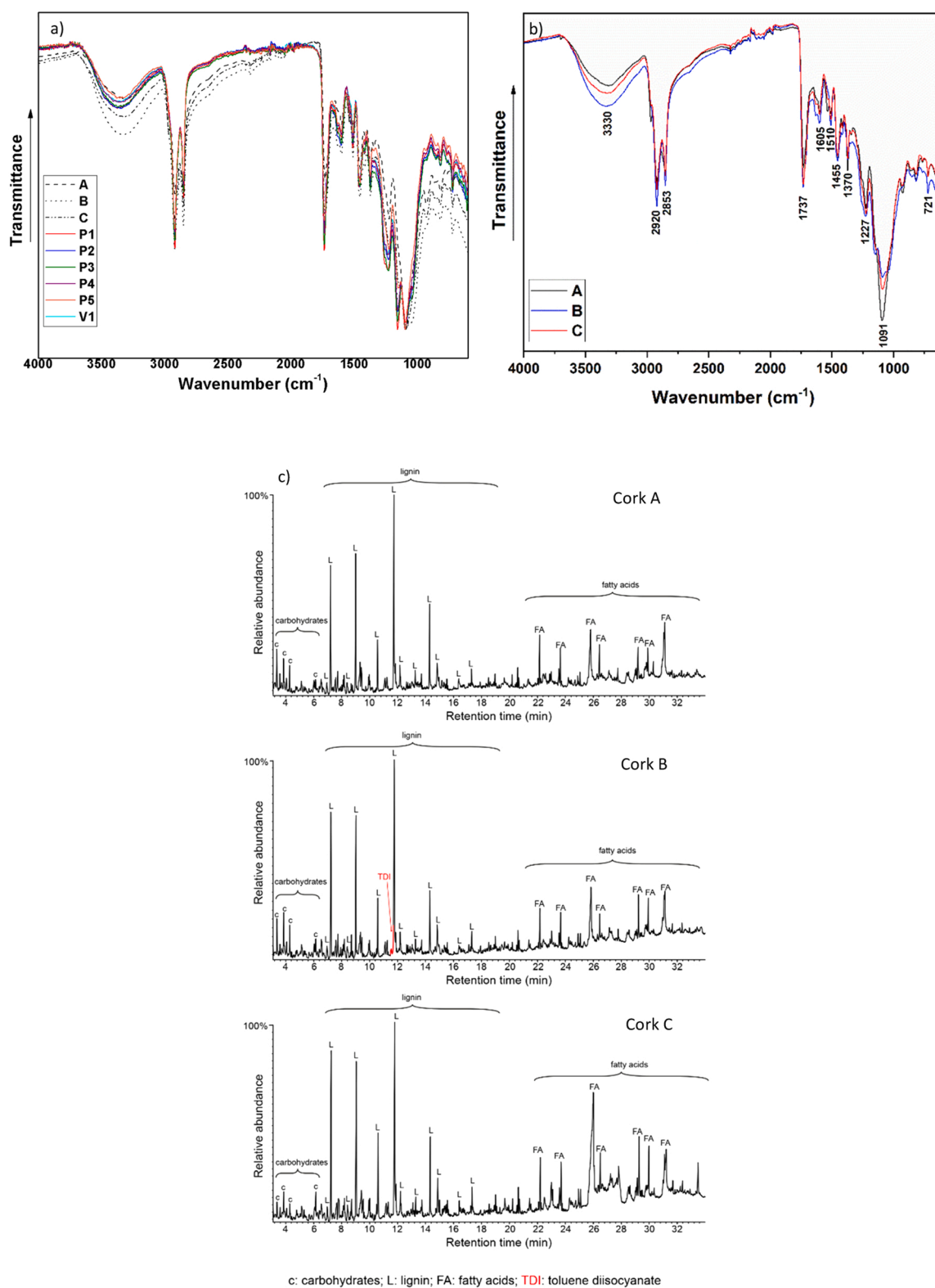**Fig. 1.** Results of the FTIR / ATR analysis. a) Comparative spectra of samples A, B, C, P1, P2, P3, P4, P5, V1. b) Spectra obtained from samples A, B, and C, where wavelength values of the main peaks are labeled. c) Results obtained from Py-GC-MS of samples A, B, and C. Main compounds released arise from carbohydrates (C), lignin (L), fatty acids (FA) from suberin. A small peak of toluene diisocyanate (TDI) is also present in cork B.

effectively determine the behavior of the AC stoppers analyzed. The aim is to form groups of samples with different behaviors for the vector of variables experimentally measured (E_c, E_t, σ_{23}, σ_{34}, σ_{50}, σ_m, ε_m, ε_{tb}, *M*, *θ*, *T*, *ε*, *D*, *H*), and to determine whether it is related to the chemical composition. The analysis was carried out by distinguishing between the replicas individually instead of using the mean value of each batch, to graphically obtain the dispersion on different replicas for a more homogeneous sampling. Additionally, it is intended to carry out a dimension reduction through factorial analysis to explain the maximum amount of information in reduced dimension (two, or a maximum of three dimensions). Finally, reduced size groups are generated and associated with a certain variable composition. The methodology is based on the Varimax-type Rotation, to obtain projections by the regression method, with a total variability explained with two factors. Complementary the discrete (P1,…, P18) nature of the variables and the different variables have different chemical compositions, prevents performing any analyses of the variance (ANOVA). The statistical calculations were performed by using the software package SPSS v.10 (IBM), under license from the University of Cádiz.

3. Results and discussion

3.1. FTIR-ATG, Py-GC-MS, and SEM analyses

Fig. 1a shows the results of FTIR-ATR analyses of the samples from stages I, II, and IV, where the different bands are associated with the presence of specific functional groups. All spectra clearly show characteristic vibrations of suberin, one of the main components of cork, as well as lignin and polysaccharides. In this way, the band around 3330 cm^{-1} is identified as stretching vibrations of O-H bonds; sharp bands at 2920 and 2853 cm^{-1} correspond to stretching vibrations of CH_2 bonds in the structure of alkyl chains; the band at 1737 cm^{-1} is assigned to stretching vibrations of C $=$ O bonds of ester groups; the band at 1605 cm^{-1} is assigned to stretching vibrations of C $=$ C bonds of aliphatic groups; the one at 1510 cm^{-1} is characteristic of the C-C bonds of aromatic rings; the band at about 1460 cm^{-1} is assigned to the aliphatic groups; the one at 1370 cm^{-1} is identified as deformation vibration of the -CH$_3$ group; the band at about 1096 cm^{-1} and the shoulder at about 1035 cm^{-1} may correspond to -CH and -CO bonds in the structure of polysaccharides that could be present in these samples; in addition to the band at about 721 cm^{-1} associated to -CH outside the suberin plane (Silva et al., 2005; Pacheco Menor et al., 2019). On the contrary, it has not been possible to observe the vibration at 2270 cm^{-1} characteristic of the isocyanate group present in toluene diisocyanate (TDI), methylene diphenylisocyanate (MDI), hexamethylene diisocyanate (HDI), and isophorone diIsocyanate (IPDI). However, the Py-GC-MS spectrum in Fig. 1b corresponding to sample B shows a characteristic peak of TDI (Sáenz-Pérez et al., 2016; Sultan et al., 2012). On the other hand, very low concentration of trichloroanisole (TCA), hindering its detection (Garcia, Lopes, Barros, De, & Ilharco, 2015), the presence of TCA can be inferred in the three reference samples: two bands are observed at 1417 cm^{-1} and 1314 cm^{-1}, in addition to an increase in intensity in the region of 950–800 cm^{-1}.

Furthermore, an approximate quantification of the main constituents in the heterogeneous mixture of the AC is reported (Fig. 1c). The results of the peak integration areas in the Py-GC-MS spectrum of sample B (Oliveira et al., 2020), allow estimating roughly their stoichiometry by main components and abundance (Carbohydrates "cellulose": 11.7%; Lignin: 37,7%; Suberin: 50.1%; TDI: 0.50%). It must be noted that this provides a rough estimation since, for instance, part of the compounds produced during the pyrolysis are not quantified (volatile compounds, such as CO_2 and water, and char).

Similarities in the FTIR-ATG spectra from different batches can easily see (Fig. 1b), highlighting the need to analyze the samples with higher-resolution techniques to address minor discrepancies between them.

Fig. 2A) shows the SEM results obtained in the different samples (A,

B, C, and P1 at the top panel and P2, P3, P4, P5 at the bottom panel). The images included evidence of the smoothness of sample B in contrast with the others, much rougher especially at the boundaries between neighboring grains, usually plenty of cracks.

The grain size of AC, as well as their distribution, can be inferred from the lower magnification images (i.e., x32), where their boundaries are highlighted by white dashed lines. The hexagonal/pentagonal prisms conforming the cork microstructure render to hexagonal/ pentagonal (honeycomb-like) or rectangular (brick wall-like) patterns, when properly aligned, as shown in the higher magnification images in Fig. 2B. The cork cells along the axial/tangential section show rectangular cross-sections, with dimensions about 20–30 μm x 40–50 μm, and 800 nm thick walls approximately. Along the axial section, the cork cells show hexagonal and/or pentagonal cross-section, 20–30 μm wide, and 1 μm cell walls, in agreement with reference (Paiva & Magalhães, 2018).

3.2. Density and relative humidity analyses

Table 2 shows the results obtained from the apparent density analysis. Most of the samples observed are within the range of tolerances required in the wine stoppers standard and it is a decisive parameter to categorize the product in the top class. Remarkably the batch B samples, with such a homogeneous and compact microstructure, has one of the lowest densities of all the references.

Notably, the product V1 has a similar density (even slightly higher) than sample A, being smaller. The value of 336 kg·cm^{-3} obtained in the V1 product is similar to the maximum obtained by (Gama, Ferreira, & Barros-timmons, 2019) for top-class cork-based composites. All the obtained values in this study are above the top-class references, excluding those studies on natural cork (Anjos et al., 2014; Oliveira et al., 2015), not agglomerated, therefore, not comparable with cork composites such as the ones studied in the present work. The average density in all measure samples is 297 kg·cm^{-3}, very similar to that obtained by (González-Hernández et al., 2014), considering the latter with a maximum value much higher than the used in this work.

Fig. 3 shows the results obtained from the relative humidity analyses. The mean measured value considering all samples is 4.04%, lower than those reported in (González-Hernández et al., 2014; Rosa and Fortes, 1993; Rosa & Fortes, 2009). Fortunately, the lower the measured relative humidity, the better performance against fungi proliferation, lengthening the stopper self-life inside the bottle of spirits, which usually lasts much longer than other sparkling, still, or generous wines.

3.3. Mechanical and thermo–mechanical properties tests

3.3.1. Compression test

Table 3 summarizes the results from the compression tests performed in the batches belonging to the four different stages (I–IV) Fig. 4a shows the stress-strain curves up to a deformation of 70% with the averages selected for each batch in each stage.

The Young's Modulus, *E*, are in general slightly lower than those reported in the literature for similar samples and much lower than natural cork, but a significant dispersion of this parameter is observed (Rosa and Fortes, 1993; Anjos, Pereira, & Rosa, 2008; Oliveira et al., 2015).

In all cases, the curves followed the known pattern of an elastic region up to strains of approximately 5%, corresponding to the elastic bending of the cell walls, followed by a large plateau or densifying zone for strains between about 5–60% caused by the progressive buckling of the cell walls, with a subsequent steep increase of stress for higher strains with the crushing and collapse of the cells (Anjos et al., 2008, 2014). Neglecting the already mentioned differences in this work (due to the cork orientation), this behavior is common to all previously described studies involving the compression of cork samples (Anjos et al., 2008; Flores, Rosa, Barlow, Fortes, & Ashby, 1992; Gybson et al., 1981). However, slight differences are observed in the region

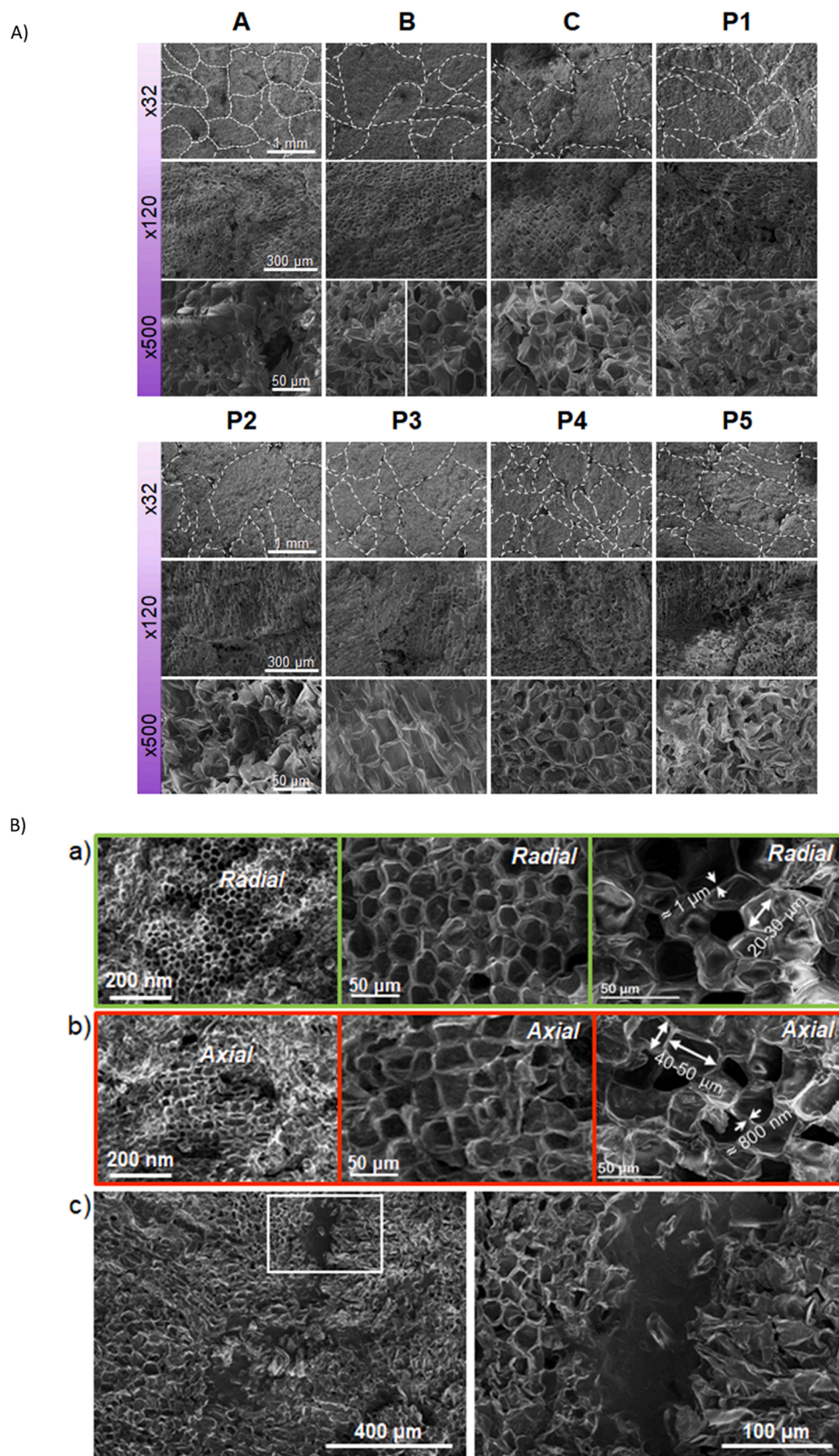**Fig. 2.** A) SEM analyses of samples: (top panel) A, B, C and P1, and (bottom panel) P2, P3, P4, and P5. First, the middle and bottom rows contain images taken at x32, x120 and x500, respectively. B) a) the radial and b) axial directions of the cork microstructure at different magnifications from stage IV samples of the product (V1) and c) detail showing the presence of TDI between two domains.

Table 2
Results obtained from the density analyses (n = 5).

| Sample	m [g]	d [mm]	l [mm]	D [kg/m³]
A	2.54	20.28	24.40	322
B	2.98	20.87	29.52	295
C	3.15	21.86	27.77	302
P1	2.70	21.00	28.00	278
P2	2.72	21.00	28.00	281
P3	2.77	21.00	28.00	286
P4	2.29	21.00	28.00	236
P5	2.61	21.00	28.00	269
P11	2.68	21.00	28.00	276
P12	2.83	21.00	28.00	292
P13	2.88	21.00	28.00	298
P14	2.84	21.00	28.00	293
P15	3.07	21.00	28.00	317
P16	3.08	21.00	28.00	318
P17	3.16	21.00	28.00	326
P18	3.21	21.00	28.00	331
P19	2.88	21.00	28.00	297
V1	2.19	18.30	26.00	336
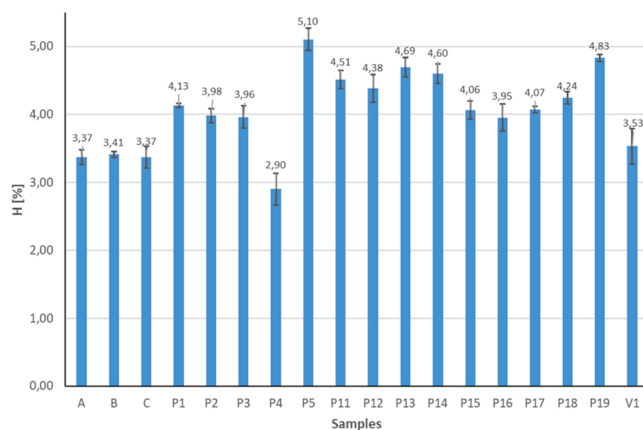
Fig. 3. Relative humidity measurements according to Spanish standards UNE 56917-88 and UNE 56922-2004.

Table 3
Results from compression tests on samples of Stages I–IV.

	Sample	E (1%–5%EL) MPa	σ_{23} MPa	σ_{34} MPa	σ_{50} MPa
Stage I	A	8.84 ± 1.33	1.15 ± 0.11	1.51 ± 0.12	2.89 ± 0.17
	B	7.12 ± 0.10	1.10 ± 0.03	1.35 ± 0.05	2.35 ± 0.11
	C	7.28 ± 0.92	0.97 ± 0.11	1.31 ± 0.13	2.52 ± 0.24
Stage II	P1	12.43 ± 1.44	0.94 ± 0.03	1.17 ± 0.04	1.70 ± 0.11
	P2	11.11 ± 1.14	0.93 ± 0.05	1.19 ± 0.07	1.73 ± 0.16
	P3	11.53 ± 0.22	0.91 ± 0.02	1.15 ± 0.03	1.68 ± 0.06
	P4	6.29 ± 1.82	0.59 ± 0.06	0.75 ± 0.08	1.06 ± 0.13
	P5	10.74 ± 0.41	0.82 ± 0.02	1.04 ± 0.02	1.50 ± 0.06
Stage III	P6	11.16 ± 0.43	1.79 ± 0.05	0.85 ± 0.02	1.06 ± 0.02
	P7	11.03 ± 0.18	1.91 ± 0.03	0.88 ± 0.02	1.1 ± 0.01
	P8	10.34 ± 0.14	1.92 ± 0.04	0.87 ± 0.01	1.1 ± 0.02
	P9	10.83 ± 0.36	1.94 ± 0.13	0.90 ± 0.05	1.13 ± 0.06
	P10	11.69 ± 0.77	2.39 ± 0.12	1.03 ± 0.04	1.32 ± 0.06
	P11	10.80 ± 0.33	2.18 ± 0.05	0.95 ± 0.02	1.21 ± 0.03
	P12	11.82 ± 0.39	2.19 ± 0.05	0.96 ± 0.01	1.21 ± 0.02
	P13	11.48 ± 0.66	2.31 ± 0.01	1.00 ± 0.00	1.28 ± 0.00
	P14	11.44 ± 0.42	2.14 ± 0.05	0.97 ± 0.01	1.23 ± 0.02
Stage IV	V1	9.25 ± 3.00	1.06 ± 0.06	1.49 ± 0.11	3.48 ± 0.88

determined by the final part of the plateau and the starting of the cell collapsing area: larger resilience and ductility are observed from 50% strain an in the already mentioned references. This is due to the composite nature of the AC used in this work compared to the natural cork used in the references. The observed behavior in Fig. 4a is similar to reference (Jardin, Fernandes, Pereira, Sousa, & De, 2015) in the case of AC, accounting for the higher densities and constant granulometry (between 0.5 and 2.0 mm) reported. A relationship between density and Young's modulus is also addressed, less dense samples leave the densification zone earlier, as previously observed by (Anjos et al., 2014). Regarding the stress values at 23%, 34% and 50% of strain, the results are good agreement with reference (Lagorce-Tachon et al., 2015), that is, there is an increase in the stress values at the indicated strains is notably accentuated in the densest batches (i.e., V1, with the highest density, reaches 3.48 Mpa at 50% of strain).

In this sense, (Silva et al., 2005) compared cork with other viscoelastic materials such as Poliurethane (PU) or Polyethylene (PE) foams (Hamdi & Mighri, 2018; Pfretzschner & Rodriguez, 1999), representing on a map the relationship between specific modulus (E/ρ) and compressive resistance (σ/ρ). Fig. 4b reproduces this map including all the batches tested (blue dots within the cork region). Sample V1 is de only one that is close to the stage I reference samples, highlighting its quality as a top-class final product.

3.3.2. Tensile test

Table 4 summarizes the results derived from the tensile tests, classified by stages, in which four parameters are presented: maximum strength (σ_m), deformation at strength (ε_m), Young's modulus in tensile (E_t) and, strain at break (ε_{tb}).

All the maximum strength values are larger than the ones observed by (Silva et al., 2005) for insulation cork agglomerate. Furthermore, the reference batch B is the one that offers the best performance in this type of tests, since it manages to reach more than half its length until breaking, similar to (Gama et al., 2019). Fig. 5a show product V1 also renders a nice performance, reaching a value close to 41% strain at break.

3.3.3. Torque test

Samples were also analyzed under torsion tests conditions in order to determine the maximum stress, and angle of torsion that can be applied before rupture. The observed breaking behavior during rotational tests is similar in all the studied samples, break from the center and showing irregular surfaces due to the alveolar structure of the cork. The resulting curves obtained from torsion tests are shown in Fig. 5b, where the evolution of torsion angle is plotted as a function of torque, and the strain percentage of samples has been determined under exposure to shear stress. Moreover, Table 5 summarizes the characteristic torsional parameters obtained from both curves.

It is evident from Fig. 5b that a similar behavior based on three well-differentiated stages can be detected for all the studied AC samples, which was characterized by an early elastic deformation (linear zone) followed by a non-linear increase in the torsion torque when raising the rotation angle and with the sample rupture occurring at the maximum torsion torque, which produced a noticeable decrease in its values.

Sample V1, chosen as a commercial product, shows the highest maximum torque and torsion angle apart from the reference samples (Table 5), in agreement with increased compaction as shown by the microstructural analyse of the AC samples.

On the other hand, the Young modulus and maximum percentage of strain are determined through stress-strain curves, providing a further measurement of the compaction degree, related to the elongation capacity. Although sample V1 showed the highest deformation degree before rupture as compared to the references materials (Table 5), it exhibited slightly lower values of the maximum stress in relation to sample B, indicating a decrease in the torsional strength.

Moreover, according to the Young Modulus calculated from the slope of the early linear zone, a remarkable difference was detected between sample V1 (E_{V1} = 31.82 MPa) compared to the reference materials (E_A = 25.81 MPa, E_B = 29.02 MPa, E_C = 24.9 MPa). Note the increased slope obtained for the elastic zone, thus indicating a higher rigidity of
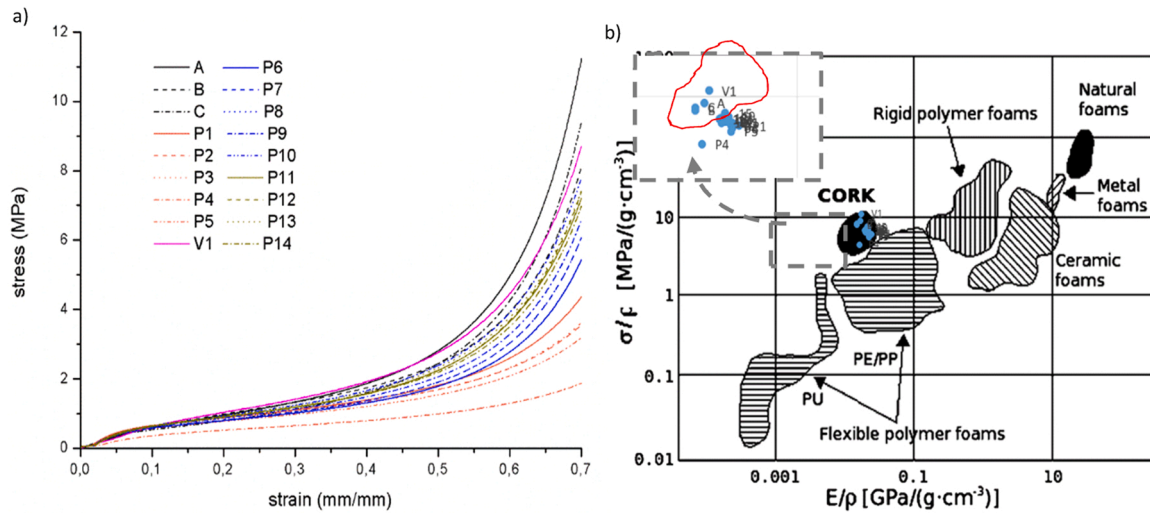
Fig. 4. a) Stress-strain curves at compression tests. B) Parametric representation map between the specific module and the specific resistance. Adapted from Silva et al. (2005).

Table 4
Results of the tensile tests on the samples (Stages I–IV).

Samples	σ_m MPa	ε_m %	E_t MPa	ε_{tb} %
A	0.94 ± 0.07	27.20 ± 6.0	13.20 ± 0.41	37.00 ± 4.0
B	0.82 ± 0.09	43.20 ± 6.0	10.46 ± 1.13	53.00 ± 4.0
C	0.78 ± 0.09	27.90 ± 3.0	9.18 ± 2.31	35.60 ± 5.0
P1	0.70 ± 0.08	23.60 ± 1.6	10.14 ± 1.09	32.40 ± 2.1
P2	0.74 ± 0.03	23.30 ± 6.1	10.96 ± 0.57	32.60 ± 5.5
P3	0.81 ± 0.03	30.40 ± 0.02	13.28 ± 0.32	38.20 ± 2.3
P4	0.53 ± 0.10	24.90 ± 4.6	7.50 ± 1.08	29.60 ± 4.9
P5	0.65 ± 0.04	17.30 ± 2.0	13.60 ± 0.58	24.00 ± 0.5
P6	0.97 ± 0.09	25.50 ± 2.0	11.22 ± 3.13	34.20 ± 4.0
P7	1.11 ± 0.08	28.00 ± 3.0	11.70 ± 0.66	34.40 ± 2.0
P8	0.97 ± 0.04	26.80 ± 2.0	11.35 ± 1.35	31.60 ± 3.0
P9	0.99 ± 0.03	28.00 ± 3.0	11.62 ± 2.48	35.70 ± 5.0
P10	0.89 ± 0.01	31.10 ± 2.0	10.91 ± 1.28	36.50 ± 2.0
P11	0.91 ± 002	31.70 ± 3.0	10.83 ± 0.84	37.90 ± 0.0
P12	0.89 ± 0.07	30.90 ± 3.0	10.45 ± 1.54	36.00 ± 3.0
P13	1.04 ± 0.06	38.30 ± 7.0	11.43 ± 1.38	45.80 ± 5.0
P14	0.94 ± 0.00	28.00 ± 2.0	15.16 ± 0.5	34.80 ± 4.0
V1	1.02 ± 0.08	34.80 ± 9.0	11.41 ± 1.02	40.90 ± 6.0

Table 5
Torsional parameters of different cork samples (according to the study phases).

| Samples	M daN cm	Θ (4 rpm) grades	T daN/cm^2	ε %
A	0.25 ± 0.01	188.46 ± 10.70	9.78 ± 0.66	171.55 ± 9.50
B	0.33 ± 0.02	200.65 ± 8.23	12.75 ± 0.84	182.45 ± 7.62
C	0.26 ± 0.01	166.23 ± 19.21	10.20 ± 0.67	151.11 ± 17.46
P1	0.16 ± 0.12	115.93 ± 7.16	6.34 ± 0.47	105.55 ± 6.60
P2	0.16 ± 0.06	152.22 ± 7.16	6.08 ± 0.21	138.56 ± 6.60
P3	0.16 ± 0.15	142.67 ± 27.54	6.35 ± 0.59	129.75 ± 24.99
P4	0.17 ± 0.02	166.73 ± 38.44	6.45 ± 0.07	151.76 ± 34.92
P5	0.25 ± 0.11	193.47 ± 4.30	9.72 ± 0.44	175.96 ± 3.81
P6	0.16 ± 0.01	185.88 ± 15.07	6.30 ± 0.28	169.12 ± 13.74
P7	0.18 ± 0.00	187.30 ± 34.98	6.86 ± 0.14	170.24 ± 31.79
P8	0.20 ± 0.02	178.59 ± 70.34	7.66 ± 0.71	162.32 ± 63.93
P9	0.19 ± 0.01	197.47 ± 16.56	7.26 ± 0.46	179.49 ± 15.05
P10	0.18 ± 0.03	181.49 ± 22.96	7.17 ± 1.05	164.96 ± 20.87
P11	0.19 ± 0.02	260.98 ± 79.03	7.55 ± 0.83	229.65 ± 66.89
P12	0.22 ± 0.02	260.32 ± 49.48	8.61 ± 0.80	232.29 ± 41.59
P13	0.20 ± 0.02	214.90 ± 35.80	7.89 ± 0.85	195.33 ± 32.54
P14	0.17 ± 0.01	161.16 ± 23.19	6.54 ± 0.33	146.48 ± 21.08
V1	**0.24 ± 0.03**	**235.24 ± 41.28**	**9.13 ± 1.34**	**213.81 ± 37.51**
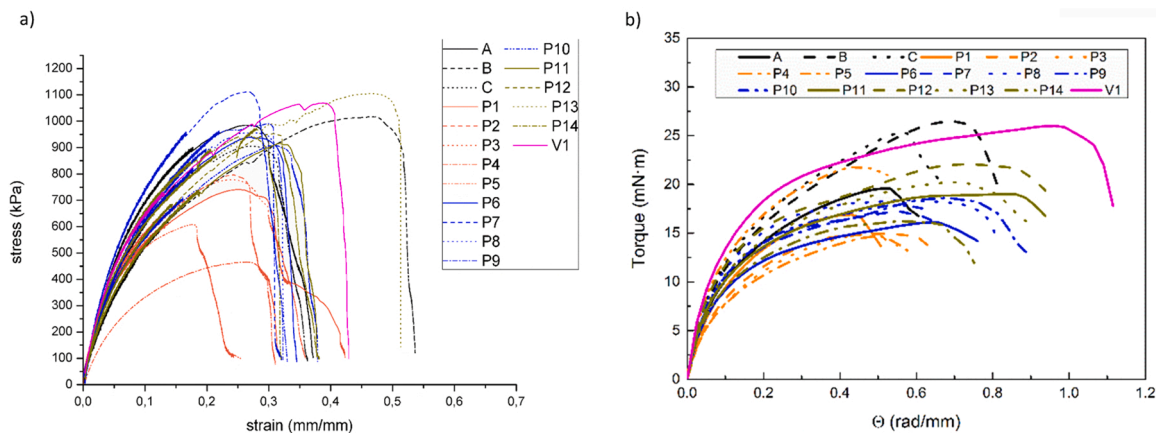
Fig. 5. a) Stress-strain curves at tensile tests. B) Torsion tests curves for AC samples (Stages I–IV), determining the evolution of both torsion angles per unit length as a function of torsion torque.

this sample and confirming the results attained with the other mechanical tests.

3.3.4. Dynamic thermo-mechanical test

The thermo-mechanical and rheological properties at the temperature range between −100 and 100 ºC are shown in Fig. 6a. The thermograms reveal two different transitions. The first one corresponds to the glass transition temperature of the polyurethane adhesive around −45 ºC (Paiva & Magalhães, 2018) whereas the second one, around 20 ºC in tanδ is found, which corresponds to the glass transition temperature of the suberin (Mano, 2002). This phenomenon is better explained by the degradation process that occurred in DSC at 3 ºC (Fig. 6c). The peak at 66 ºC may be associated with the fusion of the wax components from the manufacturing process of the stoppers and the loss of water that hardens the material and causes the increase in tanδ (Dionísio et al., 1995).

The loss of water is corroborated in the ATG (Fig. 6b), as a small drop in the weight of the sample is observed and located in the 50 ºC interval. Despite the anisotropic properties of AC, it is possible to find similarities within a temperature range, for example from 60 ºC that is when the base material is annealed. At that point, an increase in tanδ begins, which is evidenced in the curve of the derivative shown in Fig. 6b (black curve) and obtained through the thermogravimetric analysis performed in sample V1. This process is also confirmed by the thermogram represented in Fig. 6c, as a mass loss (blue curve) present around 65 ºC and resulting from the differential calorimetry test (DSC) can be distinguished.

The curves corresponding to the loss modulus (tanδ) start at −100 ºC and their magnitude allows assessing the viscoelastic behavior of the material at such temperature. Between the 3 commercial batches analyzed, B, shows the best performance, with the lowest tanδ. Surprisingly, the behavior of V1 is even better, according to the tanδ results. Identical behavior of the three references, A, B, C (Stage I), is observed

throughout the test interval, and of the 5 tested prototypes (Stage II), exhibiting all of them similar viscoelastic properties. Thus, all the samples keep their elastic properties around 15 ºC, being this factor crucial as it imposes the operating temperature of the AC stoppers for spirits.

3.4. Factorial analysis

Results were finally evaluated by Multivariate statistical analyses (Song, Wrona, Nerin, Lin, & Zhong, 2019). Correlations with a high level of significance are those with a predictable dependency relationship, such as the stress at 34% deformation in tensile tests (related to that at 50%), or the deformation in the Resistance, related to the break during compression tests (Table 6). Correlations found between the variables considered in the torsion test are even higher, as also expected.

The FA method (Mulaik, 2009), allows to group all the variables measured into 3 sets delimited by factors 1 and 2, with an explanatory

Table 6
Selection of correlations between variables according to their degree of significance.

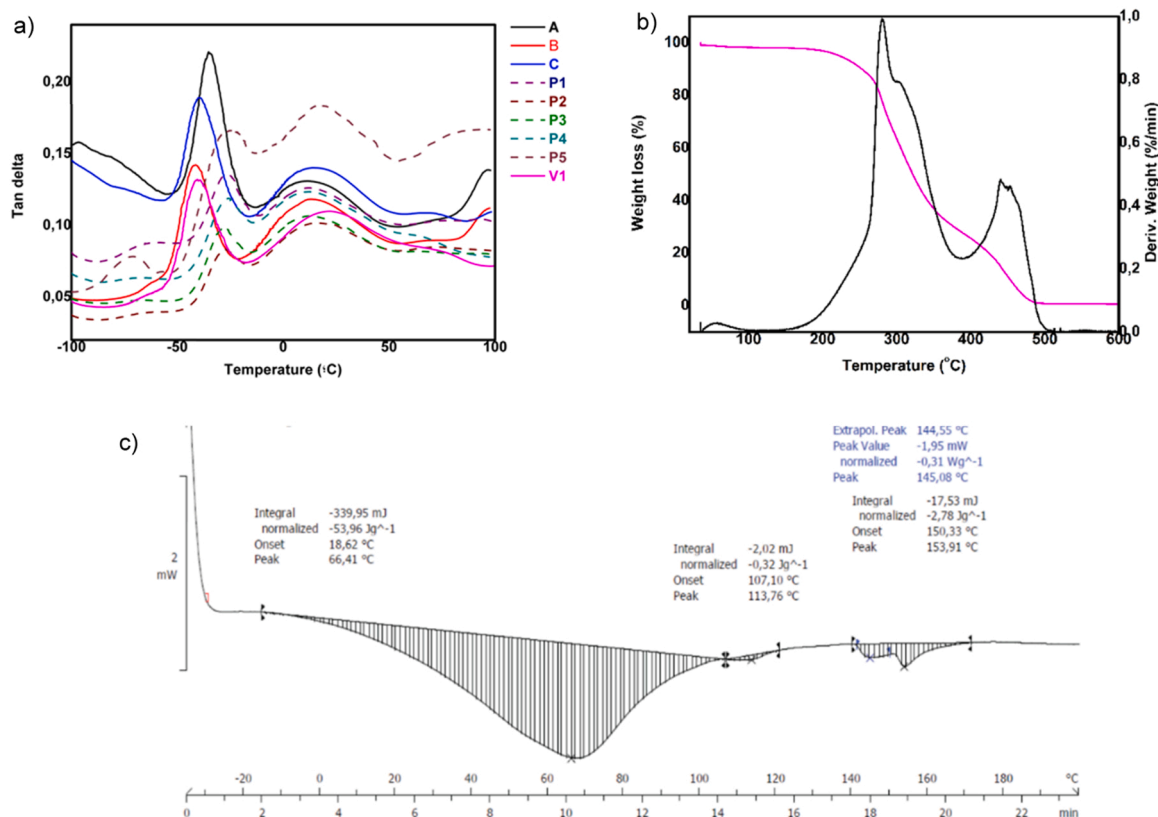|	σ_{50}	ε_{tb}	T	ε
σ_{34}	0.937			
Pearson correlation	56			
N				
ε_m		0.914		
Pearson correlation		56		
N				
M			0.999	
Pearson correlation			90	
N				
θ				0.995
Pearson correlation				90
N				

Fig. 6. a) Thermograms DMTA; b) Thermographic Analyses (TGA) of the V1 sample; c) Thermograms DSC of the V1 sample.

level of 50%, approximately. These groups of variables are categorized according to their level of explanatory importance as follows:

- GROUP 1: σ_{23}, σ_{34}, σ_{50}, M, T; (first-order variables that mainly contribute to explain the results of the tests carried out with the cork batches and aimed at assessing their differential behavior).
- **GROUP 2: σ_m, ε_m, ε_{tb}, D; (secondary variables that explain 65% of the multivariate behavior of cork).**
- GROUP 3: Ec, Et, H; (variables with the least information content to explain the multivariate behavior of the cork).

These results suggest that for successive exploratory replicates, only the variables corresponding to Groups 1 and 2 should be measured. Likewise, the results indicate the weak dependence of the Young's Modulus with compression and traction as compared to the others. Based on the presentation of the samples in factorial dimensions 1 and 2 shown in Fig. 7, samples with composition = 8 and composition = 1,2,3,18 show distinguished behavior than the other of tested compositions.

The factorial scores of the experimental measurements and their group behavior, labeled according to the explored variable "composition" reveal the homogeneity between the variables in all the experiments except AC samples with compositions 7, 8, and 16. Sample 8 presents a composition pattern different from the other two major groups, suggesting different composition despite measurements seem to be correct according to their proximity to each other. In the case of samples 1, 2, 3, and 18, it is especially relevant the correlation found between the 3 commercial batches (Stage I) and the last prototype that has currently become the first commercial product in the market.

4. Conclusions

The production process of AC stoppers for spirits and still wines involves the manufacture of an agricultural composite obtained from a natural raw material mixed with a thermoplastic system to produce a quality product that meets the standards of the wine sector packaging. To check the validity of potential products oriented for stoppers, a deep analysis of 3 international reference samples with unknown compositions has been performed. A deep series of physico-chemical analyses does not reveal meaningful differences in the composition of the samples both, macro and microstructural scales, to correlate with the differentiated behavior. Complementary, mechanical tests provide a better understanding of the static and dynamic behavior of the corks in an incremental regime of temperatures. Torsion tests valuable to assess some tested variables were particularly valuable to assess some tested variables relevant despite they scarcely reported. Nevertheless, they turned out to be significant for a better characterization of the material. This study, using 18 sample batches, analyzing 14 different physical-mechanical variables, and performing a multivariate analysis, revealed that only 5 selected variables achieve a level of knowledge of 50%. Moreover, the factorial analysis shows that sample V1, the only prototype placed in the market, is similar in a multivariate way to the 3 reference samples. This confirms the validity of both the test method and the statistical analysis, while pointing out the expected performance of the new product in the market, evolving according to the law of supply and demand.

CRediT authorship contribution statement

M. Suffo: Conceptualization, Formal analysis, Investigation, Methodology, Software, Validation, Writing – original draft, Writing – review & editing, Project administration. **D.L. Sales:** Conceptualization, Data curation, Formal analysis, Methodology, Investigation, Software, Validation, Writing – review & editing. **E. Cortés-Triviño:** Conceptualization, Data curation, Formal analysis, Methodology, Software, Investigation, Validation, Writing – review & editing. **M. de la Mata:**
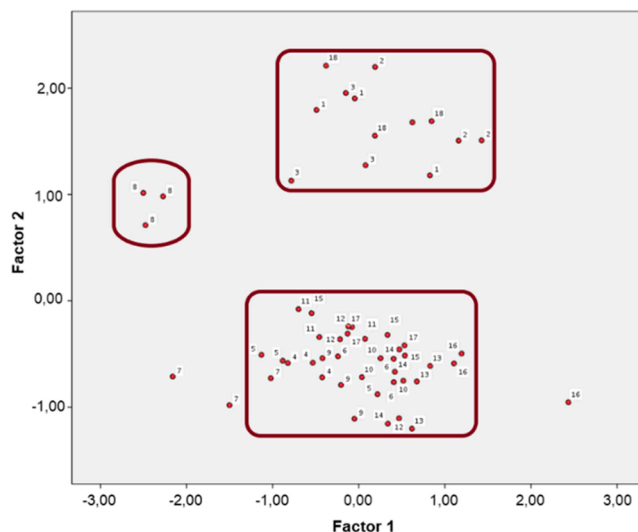

Fig. 7. Map of similarities between sample batches.

Conceptualization, Data curation, Formal analysis, Methodology, Software, Validation, Writing – review & editing. **E. Jiménez:** Conceptualization, Methodology, Resources, Writing – original draft, Supervision.

Declarations of interest

None.

Acknowledgments

References

aecork (2017). https://aecork.com/wp-content/uploads/2017/10/20140717-CIPT-v-6-.06-ESP.pdf. (Accessed 14 November 2021).

Anjos, O., Pereira;, H., & Rosa. (2010). Characterization of radial bending properties of cork. *European Journal of Wood and Wood Products*. https://doi.org/10.1007/s00107-010-0516-9

Anjos, Ofélia, Pereira, H., & Rosa, M. E. (2008). Effect of quality, porosity and density on the compression properties of cork. *Holz Als Roh - Und Werkstoff, 66*(4), 295–301. https://doi.org/10.1007/s00107-008-0248-2

Anjos, Ofélia, Pereira, H., & Rosa, M. E. (2011). Characterization of radial bending properties of cork. *European Journal of Wood and Wood Products, 69*(4), 557–563. https://doi.org/10.1007/s00107-010-0516-9

Anjos, Ofélia, Rodrigues, C., Morais, J., & Pereira, H. (2014). Effect of density on the compression behaviour of cork. *Materials and Design, 53*, 1089–1096. https://doi.org/10.1016/j.matdes.2013.07.038

Delucia, M., Catapano, A., Montemurro, M., & Pailhés, J. (2020). A stochastic approach for predicting the temperature-dependent elastic properties of cork-based composites. *Mechanics of Materials, 145*, Article 103399. https://doi.org/10.1016/j.mechmat.2020.103399

Dionísio, M. S. C., Correia, N. T., Mano, J. F., Moura Ramos, J. J., Fernandes, A. C., & Saramago, B. (1995). Absorbed water in the cork structure. A study by thermally stimulated currents, dielectric relaxation spectroscopy, isothermal depolarization experiments and differential scanning calorimetry. *Journal of Materials Science, 30*(17), 4394–4400. https://doi.org/10.1007/BF00361523

Fernandes, E. M., Correlo, V. M., Mano, J. F., & Reis, R. L. (2014). Cork-polymer biocomposites: mechanical, structural and thermal properties. *Materials and Design, 82*, 282–289. https://doi.org/10.1016/j.matdes.2015.05.040

Flores, M., Rosa, M. E., Barlow, C. Y., Fortes, M. A., & Ashby, M. F. (1992). Properties and uses of consolidated cork dust. *Journal of Materials Science, 27*(20), 5629–5634. https://doi.org/10.1007/BF00541634

Franken, U., Primke, H., & Alvaro, C. (2003). (12) Patent Application Publication (10) Pub. No.: US 2003 / 0124222 A1 Patent Application Publication. In Optics Express.

Gama, N., Ferreira, A., & Barros-timmons, A. (2019). 3D printed cork/polyurethane composite foams. *Materials & Design, 179*, Article 107905. https://doi.org/10.1016/j.matdes.2019.107905

Gameiro, C. P., Cirne, J., Gary, G., & Al, E. (2005). Numerical and experimental study of the dynamic behaviour of cork. *Des Use Light-Weight Mater*, 65–84.

Garcia, A. R., Lopes, L. F., Barros, R. B., De, & Ilharco, L. M. (2015). The problem of 2,4,6-trichloroanisole in cork planks studied by attenuated total reflection infrared spectroscopy: proof of concept. *Journal of Agricultural and Food Chemistry, 63*(1), 128–135. https://doi.org/10.1021/jf503309a

Gil, L. (2009). Cork composites: a review. *Materials, 2*(3), 776–789. https://doi.org/10.3390/ma2030776

Gil, L. (2015). New cork-based materials and applications. *Materials, 8*(2), 625–637. https://doi.org/10.3390/ma8020625

González-Hernández, F., González-Adrados, J. R., García De Ceca, J. L., & Sánchez-González, M. (2014). Quality grading of cork stoppers based on porosity, density and elasticity. *European Journal of Wood and Wood Products, 72*(2), 149–156. https://doi.org/10.1007/s00107-013-0760-x

Guillemonat, A. (1960). Progrès récents dans l'etude de la constitution chimique du liège. *Annals of Faculty of Science, 30*, 43–54.

Gybson, L. J., Easterling, K. E., & Ashby, M. F. (1981). The structure and mechanics of cork. *Proceedings of the Royal Society of London, A*(377), 99–117.

Hamdi, O., & Mighri, F. (2018). Optimization of the cellular morphology of biaxially stretched thin polyethylene foams produced by extrusion film blowing. July. doi: 10.1177/0262489318797517.

Hejnowicz, Z., & Sievers, A. (1996). Tissue stresses in organs of herbaceous plants – III. Elastic properties of the tissues of sunflower hypocotyl and origin of tissue stresses. *Journal of Experimental Botany, 47*(297), 519–528. https://doi.org/10.1093/jxb/47.4.519

Jardin, R. T., Fernandes, F. A. O., Pereira, A. B., Sousa, R. J. A., & De. (2015). Static and dynamic mechanical response of different cork agglomerates. *Journal of Material & Design, 68*, 121–126. https://doi.org/10.1016/j.matdes.2014.12.016

Lagorce-Tachon, A., Karbowiak, T., Champion, D., Gougeon, R. D., & Bellat, J. P. (2015). Mechanical properties of cork: effect of hydration. *Materials and Design, 82*, 148–154. https://doi.org/10.1016/j.matdes.2015.05.034

Mano, J. F. (2002). The viscoelastic properties of cork. *Journal of Materials Science, 37*(2), 257–263. https://doi.org/10.1023/A:1013635809035

Mestre, A., & Vogtlander, J. (2013). Eco-efficient value creation of cork products: an LCA-based method for design intervention. *Journal of Cleaner Production, 57*, 101–114. https://doi.org/10.1016/j.jclepro.2013.04.023

Mulaik, S. A. (2009) (second ed.). *Statistics in the Social and Behavioral SciencesFoundations of Factor Analysis*. Chapman & Hall/CRC. https://doi.org/10.1201/b15851

Natividade, J. V. (1950). *Subericultura*. Ministerio da Economia. Direcção-Geral Servicios Florestais e Aquicolas.

Oliveira, A. S., Furtado, I., Bastos, M. L., Guedes de Pinho, P., & Pinto, J. (2020). The influence of different closures on volatile composition of a white wine. September 2019 *Food Packaging and Shelf Life, 23*. https://doi.org/10.1016/j.fpsl.2020.100465.

Oliveira, V., Knapic, S., & Pereira, H. (2015). Classification modeling based on surface porosity for the grading of natural cork stoppers for quality wines (November) *Food and Bioproducts Processing, 93*, 69–76. https://doi.org/10.1016/j.fbp.2013.11.004.

Pacheco Menor, M. C., Serna Ros, P., Macías García, A., & Arévalo Caballero, M. J. (2019). Granulated cork with bark characterised as environment-friendly lightweight aggregate for cement based materials. *Journal of Cleaner Production, 229*, 358–373. https://doi.org/10.1016/j.jclepro.2019.04.154

Paiva, D., & Magalhães, F. D. (2018). Dynamic mechanical analysis and creep-recovery behavior of agglomerated cork. *European Journal of Wood and Wood Products, 76*(1), 133–141. https://doi.org/10.1007/s00107-017-1158-y

Pereira, H. (1988). Chemical composition and variability of cork from Quercus suber L. *Wood Science and Technology, 22*(3), 211–218. https://doi.org/10.1007/BF00386015

Pereira, H. (2011). *Cork: Biology, Production and Uses*. Elsevier.

Pérez-Terrazas, D., González-Adrados, J. R., & Sánchez-González, M. (2020). Qualitative and quantitative assessment of cork anomalies using near infrared spectroscopy (NIRS) (February) *Food Packaging and Shelf Life, 24*, Article 100490. https://doi.org/10.1016/j.fpsl.2020.100490.

Pfretzschner, J., & Rodriguez, R.M. (1999). Acoustic properties of rubber crumbs. 18, 81–92.

Policarpo, H., Neves, M. M., & Maia, N. M. M. (2014). On a hybrid analytical-experimental technique to assess the storage modulus of resilient materials using symbolic computation. *Journal of Symbolic Computation, 61–62*(1), 31–52. https://doi.org/10.1016/j.jsc.2013.10.007

Rives, J., Fernandez-Rodriguez, I., Rieradevall, J., & Gabarrell, X. (2011). Environmental analysis of the production of natural cork stoppers in southern Europe (Catalonia - Spain). *Journal of Cleaner Production, 19*(2–3), 259–271. https://doi.org/10.1016/j.jclepro.2010.10.001

Rives, J., Fernández-Rodríguez, I., Rieradevall, J., & Gabarrell, X. (2012). Environmental analysis of the production of champagne cork stoppers. *Journal of Cleaner Production, 25*, 1–13. https://doi.org/10.1016/j.jclepro.2011.12.001

Rocha, S. M., Ganito, S., Barros, A., Carapuça, H. M., & Delgadillo, I. (2005). Study of cork (from Quercus suber L.)-wine model interactions based on voltammetric multivariate analysis. *Analytica Chimica Acta, 528*(2), 147–156. https://doi.org/10.1016/j.aca.2004.10.001

Rosa, M., & Fortes, M. (1993). Water absorption by cork. *Wood and Fiber Science, 25*(4), 339–348. https://doi.org/http://swst.metapress.com/content/120742/.

Rosa, M. E., & Fortes, M. A. (2009). Recovery of used cork stoppers. *Colloids and Surfaces A: Physicochemical and Engineering Aspects, 344*(1–3), 97–100. https://doi.org/10.1016/j.colsurfa.2009.02.035

Sáenz-Pérez, M., Lizundia, E., Laza, J. M., García-Barrasa, J., Vilas, J. L., & León, L. M. (2016). Methylene diphenyl diisocyanate (MDI) and toluene diisocyanate (TDI) based polyurethanes: thermal, shape-memory and mechanical behavior. *RSC Advances, 6*(73), 69094–69102. https://doi.org/10.1039/C6RA13492K

Sánchez-González, M., & Pérez-Terrazas, D. (2018). Assessing the percentage of cork that a stopper should have from a mechanical perspective (July) *Food Packaging and Shelf Life, 18*, 212–220. https://doi.org/10.1016/j.fpsl.2018.10.009.

Silva, S. P., Sabino, M. A., Fernandas, E. M., Correlo, V. M., Boesel, L. F., & Reis, R. L. (2005). Cork: properties, capabilities and applications. *International Materials Reviews, 50*(6), 345–365. https://doi.org/10.1179/174328005X41168

Song, X. C., Wrona, M., Nerin, C., Lin, Q. B., & Zhong, H. N. (2019). Volatile non-intentionally added substances (NIAS) identified in recycled expanded polystyrene containers and their migration into food simulants (April) *Food Packaging and Shelf Life, 20*, Article 100318. https://doi.org/10.1016/j.fpsl.2019.100318.

Sultan, M., Zia, K. M., Bhatti, H. N., Jamil, T., Hussain, R., & Zuber, M. (2012). Modification of cellulosic fiber with polyurethane acrylate copolymers. Part I: physicochemical properties. *Carbohydrate Polymers, 87*(1), 397–404. https://doi.org/10.1016/j.carbpol.2011.07.070

Urion, K. C., Bellat, J. P., Liger-Belair, G., Gougeon, R. D., & Karbowiak, T. (2021). Unravelling CO_2 transfer through cork stoppers for Champagne and sparkling wines (November 2019) *Food Packaging and Shelf Life, 27*. https://doi.org/10.1016/j.fpsl.2020.100618.

Xu, X., Huang, G., Liu, L., & He, C. (2019). A factorial environment-oriented input-output model for diagnosing urban air pollution. *Journal of Cleaner Production, 237*, Article 117731. https://doi.org/10.1016/j.jclepro.2019.117731